Density dependence of the atomic transition probabilities in hot, dense plasmas

D. Salzmann and H. Szichman
Department of Plasma Physics, Department of Plasma, Soreq Nuclear Research Center, Yavne 70600, Israel
(Received 18 June 1986)

The atomic properties and transition probabilities of highly ionized aluminum in hot, dense plasmas were studied. In particular, we present computational results of the variations with density of the following atomic parameters: atomic potential and screening factor (due to both bound and free electrons), free-electron distribution, atomic wave functions, binding energies, line shifts, and, finally, transition probabilities and oscillator strengths. The calculations were carried out using the ion-sphere model (ISM) which treats the bound and free electrons in the atom self-consistently in a central potential. This potential is produced by the combination of the nuclear Coulomb field together with contributions by the bound- and free-electron charge distributions. The results indicate an increasing effect of the plasma on the atomic properties with increasing plasma density. Particularly, the free-electron screening reduces the atomic potential, pushes the atomic wave functions away from the nucleus, and reduces the binding energy of the bound electrons. The transition probability also decreases monotonically with density up to the ionization limit of the upper state beyond which it drops to zero. The computational results are compared to those expected from a homogeneous free-electron spatial distribution.

I. INTRODUCTION

The effort concentrated in recent years on the research into hot, dense plasmas, particularly astrophysical and laser-produced plasmas, has stimulated extensive theoretical and experimental investigation of the atomic processes in these plasmas. Of central interest in this research are the attempts to calculate the energy levels and the cross sections of the various atomic processes of highly ionized species present in hot plasmas.[1] From the results of these calculations one can gain information about the charge-state distribution as well as the radiation spectrum and radiation rates.

In this paper we study the variations of the atomic transition probabilities (the Einstein A coefficients) and the oscillator strengths versus density and temperature in hot, dense plasmas. The atomic transition probabilities and the oscillator strengths have a special importance in these plasmas because reliable calculations of these probabilities are essential for the correct description of the radiative processes in the plasma. These processes incorporate the total plasma radiation rate which determine the local plasma cooling, the computation of the plasma opacities and the Rosseland mean-free path which are of central importance in radiation transport calculations, and, finally, the calculation of the emitted radiation spectra for plasma-diagnostic purposes.

In addition to the transition probabilities we derive in this paper the density variations of a set of other quantities as well; these are the (i) atomic potentials, (ii) atomic wave functions, (iii) energy levels, (iv) free-electron distributions, and (v) chemical potentials.

While the atomic energy levels and the transition probabilities in plasmas up to $n_T < 10^{20}$ ions/cm^3 (n_T is the ion number density) can be calculated from basic principles by well-known techniques, at higher densities the surrounding plasma, namely the neighboring electrons and ions, may have a strong perturbing effect on the atomic energy levels and the wave functions of the bound electrons, thereby significantly altering the atomic transition probabilities as well as the atomic cross sections. In principle, to obtain a complete solution of such a problem one should account for the interaction of every plasma particle with every other one, but as it is impractical to carry out such a detailed computation, various approximation schemes have been proposed for this purpose.

The earliest attempt to calculate the effects of the plasma on the atomic structure is the Debye-Huckel theory,[2] appropriate for low densities, which calculates the screening of the atomic potential by the plasma particles. Other, more recent theories include the hypernetted-chain approximation,[3] the density-functional theory,[4] the Thomas-Fermi atom[1,2] and the ion-sphere model[5–7] (ISM). The first four of these models (except ISM) assume a local thermodynamic equilibrium (LTE), namely, a Boltzmann-type population distribution of the excited states. This assumption is certainly true for low-temperature plasmas. However, for every given density there are temperatures high enough so that the LTE assumption is not valid anymore.[8,9] When this limit is achieved it is expected that only a detailed-configuration-(DC) type computation can yield reasonably accurate results. The ion-sphere model can provide the framework for such a computation.

In recent years only a few attempts were made to carry out detailed-configuration-type calculations which take into account the plasma effects. A computation of the photoabsorption cross sections of an aluminum plasma in the density range of 10^{20}–3×10^{23} cm^{-3} was carried out Salzmann, Yin, and Pratt[10] who compared the plasma effects on the photoionization cross sections in a $T=500$ eV aluminum plasma as calculated within the framework of

the DC and the average-atom (AA) models. Other DC-type calculations which treat the bound and free electrons self-consistently include those by Skupsky,[11] who concentrated on the calculation of the level and line shifts in hot, dense neon plasmas, and by Davis and Blaha[12] who solved the Schrödinger equation for a single hydrogenic neon ion immersed in a fully ionized hydrogen plasma. This last paper includes a calculation of the variation with density of the level and line shifts as well as the transition probabilities and the collision strengths for the Ne X ion under several temperature and ion-density conditions. The Lyman-α line shifts versus density of the same ion were calculated recently also by Nguyen, Koenig, and Coulaud[13] using self-consistent nonrelativistic ISM.

A high-temperature pure aluminum plasma was chosen to illustrate our studies. Most of the calculations were carried out at a constant temperature of $kT=500$ eV and ion densities n_T up to 3×10^{24} cm^{-3} corresponding to a plasma coupling constant[3] Γ of 6.7 ($\Gamma=\bar{Z}^2e^2/kTR$, R is the ion-sphere radius) covering a range of transition from weak to rather strongly coupled plasmas. In this density and temperature range the plasma consists mainly of hydrogen like and heliumlike ions with a small percentage of fully ionized and lithiumlike species; therefore our calculations refer to these species only. For comparison purposes, we carried out a set of computations also for constant-density plasmas to examine the influence of temperature variations on the transition probability.

In the next section our basic model is described, and the results are presented and analyzed in Sec. III.

II. THE BASIC FORMALISM

For discussion purposes, our model can be divided into two parts: Sec. II A, computation of the atomic potential, screening factor, electron density distributions, and bound-electron wave functions and Sec. II B, calculation of the transition matrix elements, the transition probabilities, and oscillator strengths. For the sake of comparison, we list in Sec. II C the formulas relevant to plasmas with homogeneous free electron distribution.

A. The ion-sphere model calculations

We consider an ion having nuclear charge Z and ionic charge Z_f positioned at $r=0$. The number of the bound electrons ($Z_b=Z-Z_f$) as well as their distribution among the various excited states are predetermined conditions of the problem to be solved. The ion together with Z_f free electrons are confined to the ion sphere $r<R=(3/4\pi n_T)^{1/3}$, where R is the ion-sphere radius and n_T the total ion density. Beyond this sphere the distribution of the positive charge is assumed to neutralize exactly the negative electron distribution, thereby producing an electrically neutral background. Similar models, generally called ion-sphere models, were used in the literature,[5,14] sometimes with minor variations.

In our model both the bound and the free electrons are treated self-consistently in a central potential $V(r)$. More accurately, assuming some initial estimate for the free- and bound-electron charge distributions, the potential produced by these distributions is obtained from the Poisson equation,

$$\nabla^2V_e(r)=-4\pi[n_f(r)+n_b(r)]\ , \tag{1}$$

where $n_f(r)$ and $n_b(r)$ are the free- and bound-electron densities, respectively. The total potential is

$$V(r)=-Z/r+V_e(r)+V_{\rm xc}(r)\ , \tag{2}$$

where $V_{\rm xc}$ is the exchange potential, which will be discussed below.

The bound-electron eigenvalues and wave functions are obtained by solving the relativistic Dirac equation in this central potential $V(r)$

$$[-i\alpha\nabla+\beta mc^2+V(r)]\psi_{\kappa m}=E\psi_{\kappa m}\ , \tag{3}$$

where α and β are the Dirac matrices, E is the total (including rest mass) energy of the bound electron, and

$$\psi_{\kappa m}=\frac{1}{r}\begin{bmatrix} g_\kappa\Omega_{\kappa m} \\ if_\kappa\Omega_{-\kappa m}\end{bmatrix} \tag{4}$$

is the eigenfunction with the corresponding quantum numbers $\kappa=j\pm\frac{1}{2}$ and m. The radial functions $g_\kappa(r)$ and $f_\kappa(r)$ are the large and small components connected by the differential equations,

$$\begin{aligned}\frac{dg_\kappa}{dr}&=[E+mc^2-V(r)]f_\kappa(r)-\frac{\kappa}{r}g_\kappa(r)\ ,\\ \frac{df_\kappa}{dr}&=\frac{\kappa}{r}f_\kappa(r)-[E-mc^2-V(r)]g_\kappa(r)\ ,\end{aligned} \tag{5}$$

and $\Omega_{\kappa m}$ stands for the angular components of the wave function. From these wave functions the bound-electron spatial distribution can be calculated as

$$n_b(r)=\sum_\kappa(2j+1)\,|\,\psi_\kappa\,|^2\ . \tag{6}$$

In all our examples the bound-electron charge distribution outside the ion sphere was small.

The free-electron spatial distribution is assumed to follow Fermi-Dirac statistics:

$$n_f(r,\mu)=\frac{1}{2\pi^2}\left[\frac{2mkT}{\hbar^2}\right]^{3/2}F_{1/2}\left[\frac{\mu-eV(r)}{kT};\left|\frac{eV(r)}{kT}\right|\right]\ , \tag{7}$$

where $F_j(x;\beta)$ is the incomplete Fermi-Dirac function of order j defined by

$$F_j(x;\beta)=\int_\beta^\infty\frac{y^j}{\exp(y-x)+1}dy\ , \tag{8}$$

and μ is the chemical potential, which is solved numerically from the equation

$$Z_f=\int_0^R n_f(r;\mu)d^3r\ . \tag{9}$$

The solutions for the densities $n_f(r)$ and $n_b(r)$ are then substituted back into Eq. (1) to yield a better approximation for the potential $V(r)$ and the whole procedure is repeated until convergence is attained. In this sense the final potential can be regarded as self-consistent in both the

bound and free electrons.

Exchange interactions are introduced through a zero-temperature Slater-type exchange potential,

$$eV_{\rm xc}(r)=-\frac{3e^2}{4\pi}[3\pi^2 n_e(r)]^{1/3}\ , \tag{10}$$

where $n_e(r)$ is the total (bound plus free) electron density. For the calculations of the bound-electron wave functions a Latter-tail-type asymptotic behavior [for $r\to\infty$, $rV(r)\to-(Z-Z_b-Z_f-1)=-1$] was used in calculating ψ. It is expected that a Latter-tail-type boundary condition is appropriate as long as the electron orbital frequency is much higher than the plasma frequency, otherwise a time-dependent screening of the free electrons on the atomic potential should be accounted for. For the cases studied in this paper the electron orbital frequency was at least 20 times (more often 10^3 times) larger than the plasma frequency so that the Latter tail seems to be a plausible assumption. However, at present the significance of the Latter tail is still an open question and a separate research into this problem would be highly desirable.

Our calculation lacks a few ingredients, which were included in various previous work. First, the free-electron correlations[1,11,15] are neglected. These are introduced generally by means of an effective potential, but they probably have only a minor effect on the results.[11] Second, no finite-radius boundary conditions are used,[7] thereby limiting our treatment to atomic states which are not too close to the ionization limit. Finally, the neighboring-ion spatial distribution is implicitly included in the ISM by assuming a neutral background beyond the ion sphere, rather than using an explicit pair correlation function[4] (radial distribution function[3]) $g(r)$. For a very high coupling constant such a description may be inadequate, as a lattice-type structure builds up in the plasma, but for $\Gamma<7$, which is the limit of our present calculations, a homogeneous ion distribution beyond the ion sphere is still a plausible approximation.[3,4]

B. Transition probability and oscillator strength

The calculation of the transition probabilities was based on the formulas published by Grant.[16] These formulas correspond to relativistic single-particle transitions which account for the various gauge transformations of the electromagnetic field. The spontaneous transition probability per unit time from an upper state 2 to a lower state 1 is given by

$$A_{2\to1}=2\alpha\omega\left[\frac{2j_1+1}{2L+1}\right]\begin{pmatrix} j_2 & L & j_1 \\ \frac{1}{2} & 0 & -\frac{1}{2}\end{pmatrix}^2|M_{12}|^2\ , \tag{11}$$

where α is the fine-structure constant, ω is the transition frequency, $\hbar\omega=E_2-E_1$, and L is the transition multipole. The transition matrix element takes different forms for magnetic and electric transitions. For magnetic transitions,

$$M^m_{12}=i^{L+1}\frac{2L+1}{\sqrt{L(L+1)}}(\kappa_1+\kappa_2)I^+_L(\omega) \tag{12}$$

whereas for electric-type multipoles

$$M^e_{12}=M^e_{12}(0)+G_L M^l_{12}\ , \tag{13}$$

where

$$M^e_{12}(0)=i^L\left[\left[\frac{L}{L+1}\right]^{1/2}[(\kappa_1-\kappa_2)I^+_{L+1}+(L+1)I^-_{L+1}] - \left[\frac{L+1}{L}\right]^{1/2}[(\kappa_1-\kappa_2)I^+_{L-1}-LI^-_{L-1}]\right] \tag{14}$$

is the electric matrix element, and

$$M^l_{12}=i^L[(2L+1)J_L+(\kappa_1-\kappa_2)(I^+_{L+1}+I^+_{L-1}) -LI^-_{L-1}+(L+1)I^-_{L+1}] \tag{15}$$

is the longitudinal matrix element.

In formulas (12), (14), and (15) the following notation is used:

$$I^+_L(\omega)=\int_0^\infty(g_1f_2+f_1g_2)j_L\left[\frac{\omega r}{c}\right]dr\ , \tag{16}$$

$$I^-_L(\omega)=\int_0^\infty(g_1f_2-f_1g_2)j_L\left[\frac{\omega r}{c}\right]dr\ , \tag{17}$$

$$J_L(\omega)=\int_0^\infty(g_1g_2+f_1f_2)j_L\left[\frac{\omega r}{c}\right]dr\ , \tag{18}$$

j_L is the spherical Bessel function of order L.

The oscillator strength is obtained by

$$f_{1\to2}=\frac{mc^2}{2\alpha\hbar\omega^2}\left[\frac{2j_2+1}{2j_1+1}\right]A_{2\to1}\ . \tag{19}$$

The factor G_L in Eq. (13) is the gauge parameter. Grant[16] showed that for the Coulomb gauge one has $G_L=0$. For this value of G_L his results reproduce in the nonrelativistic limit the usual dipole-velocity matrix element. On the other hand, the value $G_L=[(L+1)/L]^{1/2}$, when $L=1$, corresponds to the dipole-length matrix element.

The difference between the dipole-velocity and dipole-length matrix elements depends not only on the value of G_L, but on the value of the longitudinal matrix element, M^l_{12}, Eq. (15), as well. In Ref. 16 a theorem is proved which states that this matrix element vanishes identically for all pairs of states which are eigensolutions of the same Dirac Hamiltonian. In all our calculations of the isolated hydrogenlike ion case, this condition was rigorously fulfilled. However, our calculations of the transition probabilities in high-density plasmas or complicated ions is based on the relaxed core assumption, which uses slightly different Hamiltonians for the upper and lower states. The transition probabilities, as calculated in the dipole-velocity or dipole-length cases are, therefore, not necessarily equal, and moreover, their difference is density

dependent. We shall come back to this point in the next section.

C. Homogeneous free-electron distribution

For comparison purposes we list here the formulas for the energy level shifts and line shifts which correspond to the case of a homogeneous free-electron spatial distribution throughout the ion sphere. This case can be solved analytically resulting in rather simple formulas which can be compared to the more accurate computations.

The potential produced by a homogeneous free electron distribution inside the ion sphere is

$$eV_f(r)=\frac{3Z_f e^2}{2R}\left[1-\tfrac{1}{3}\left[\frac{r}{R}\right]^2\right] . \tag{20}$$

When the radius of the ion is much smaller than the ion-sphere radius, the second term in Eq. (20) is negligible relative to 1, and Eq. (20) predicts that all the ionic energy levels are shifted upward by a constant amount, which is proportional to the density to the power $\frac{1}{3}$,

$$\delta\varepsilon=\frac{3}{2}\frac{Z_f e^2}{R}=\tfrac{3}{2}\left[\frac{4\pi}{3}\right]^{1/3} Z_f e^2 n_T^{1/3} . \tag{21}$$

Therefore, within this approximation, the emitted spectral-line energies should not be influenced by the plasma-density effects.

The line shifts are predicted as a second-order approximation, which takes into account the $(r/R)^2$ term too. The result is

$$\delta(h\nu)=-\frac{1}{2}\frac{Z_f e^2}{R^3}(\langle r_2^2\rangle-\langle r_1^2\rangle) , \tag{22}$$

where $\langle r^2\rangle$ are the average of r^2 in the upper or lower states given by,[1]

$$\begin{aligned}\langle r_{nl}^2\rangle&=\frac{a_0^2}{2Q^2}\{n^2[5n^2+1-3l(l+1)]\}\\&=\frac{a_0^2}{2Q^2}c_{nl} .\end{aligned} \tag{23}$$

Here Q is the effective charge and c_{nl} is defined as the term in the curly brackets. Substituting Eq. (23) into (22) one gets a linear dependence of the line shifts on the ion density,

$$\delta(h\nu)=-\frac{\pi}{3}\frac{Z_f}{Q^2}e^2 a_0^2 n_T(c_2-c_1) . \tag{24}$$

The minus sign indicates that the lines are shifted toward lower energies, namely, they are all red shifted. We recall that this is a second-order-approximation result and is, therefore, strongly dependent on the accuracy of the model.

The density dependence of the transition probabilities cannot be expressed by simple expressions like Eqs. (21) or (22). Second-order perturbation theory indicates that this parameter is linearly dependent on the total ion density as long as the upper level is not too close to the ionization limit,

$$\frac{\delta A_{21}}{A_{21}}=1+\alpha_{21}n_T+\beta_{21}n_T^2+\cdots . \tag{25}$$

Only near the ionization limit do the quadratic and higher-order terms come into effect. The coefficients α and β have a rather complex dependence on the isolated ion dipole and quadrupole matrix elements which connect the upper and lower states of the transition to all the other atomic levels.

III. RESULTS

Calculations were carried out for a pure aluminum plasma at $kT=500$ eV and ion densities up to 3×10^{24} cm^{-3}. The criterion in choosing the upper limit for the ion density was the requirement that the bound electron in the upper level would be confined within the ion sphere with probability greater than 90%, $\int_{r\le R}|\psi|^2 d^3r>0.9$. A set of computations was carried out also for a constant density plasma to examine the influence of temperature variations on the results. The following transitions were considered:

Al XIII, H-like:	$1s\,^2S_{1/2}-2p\,^2P_{1/2}$
	$1s\,^2S_{1/2}-2p\,^2P_{3/2}$
	$1s\,^2S_{1/2}-3p\,^2P_{1/2}$
	$1s\,^2S_{1/2}-3p\,^2P_{3/2}$
Al XII, He-like:	$1s^2\,^1S_0-1s\,2p(\frac{1}{2},\frac{1}{2})$
	$1s^2\,^1S_0-1s\,2p(\frac{1}{2},\frac{3}{2})$
	$1s^2\,^1S_0-1s\,3p(\frac{1}{2},\frac{1}{2})$
	$1s^2\,^1S_0-1s\,3p(\frac{1}{2},\frac{3}{2})$
Al XI, Li-like:	$1s^2 2s\,^2S_{1/2}-1s^2 3p\,^2P_{1/2}$
	$1s^2 2s\,^2S_{1/2}-1s^2 3p\,^2P_{3/2}$
	$1s^2 2p\,^2P_{1/2}-1s^2 3s\,^2S_{1/2}$
	$1s^2 2p\,^2P_{1/2}-1s^2 3d\,^2D_{3/2}$
	$1s^2 2p\,^2P_{3/2}-1s^2 3s\,^2S_{1/2}$
	$1s^2 2p\,^2P_{3/2}-1s^2 3d\,^2D_{3/2}$
	$1s^2 2p\,^2P_{3/2}-1s^2 3d\,^2D_{5/2}$

These transitions are, in general, the strongest in plasmas under consideration.

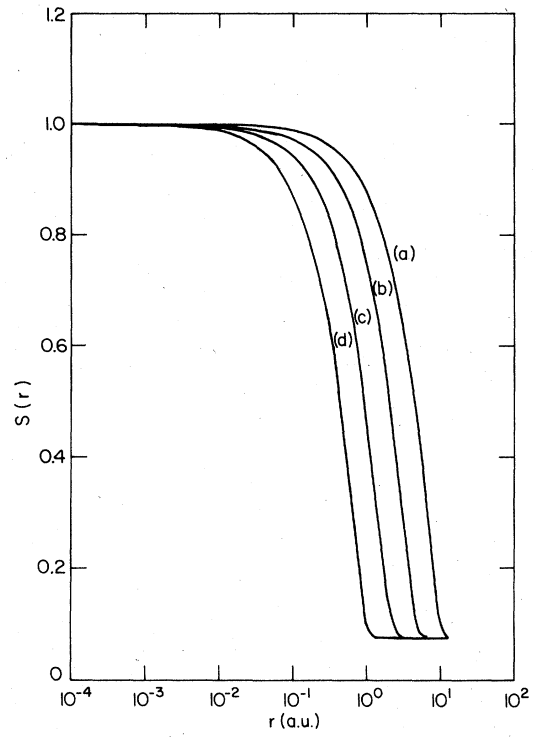

FIG. 1. Screening factor, $S(r)=-rV(r)/Z$, in a ground-state hydrogenlike ion at four ion densities: (a) 10^{21} cm^{-3}; (b) 10^{22} cm^{-3}; (c) 10^{23} cm^{-3}; and (d) 10^{24} cm^{-3}.

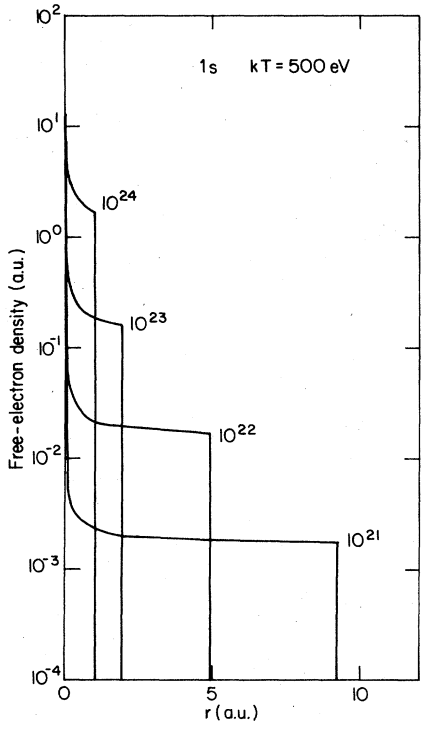

FIG. 2. Free-electron spatial distribution surrounding a ground-state hydrogenlike ion at four ion densities. Both axes are in atomic units.

A. Screening factor

In Fig. 1 we show the screening factor $S(r)=|rV(r)/Z|$ for an H-like ground-state ion at various densities. The screening factor is a monotonically decreasing function of the radius. The distance at which the screening factor is reduced to $S(r)=0.5$ is roughly proportional to the ion-sphere radius. At large distances from the nucleus the screening factor obtains the value determined by the Latter tail, $S\rightarrow 1/Z=0.0769$. We recall that the total screening factor reflects a self-consistent treatment of both the bound- and free-electron distributions as well as their mutual interaction.

B. Free-electron density distribution

The free-electron spatial distribution within the ion sphere around a ground-state H-like ion is shown in Fig. 2 at a few ion densities. Sharp polarization of the free electrons can be seen around the nucleus, while the distribution is almost homogeneous outside the ion. It can be shown that for a Fermi-Dirac distribution the transition between these two regions occurs around $r=e^2Za_0/(-\mu)$. Very close to the nucleus, the free-electron distribution is practically independent of the plasma density. This

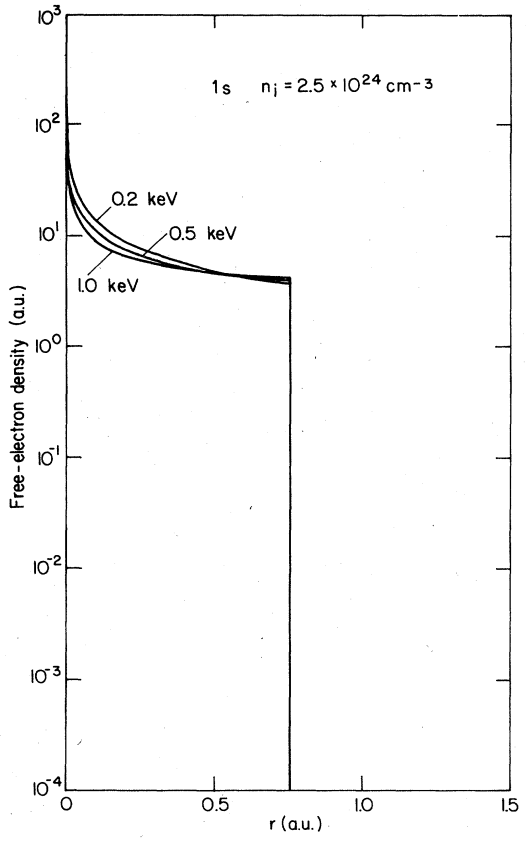

FIG. 3. Free-electron spatial distribution surrounding a ground-state hydrogenlike ion at constant ion density, $n_T=2.5\times 10^{24}$ cm^{-3}, at temperatures $T=0.2$, 0.5, and 1.0 keV. Both axes are in atomic units.

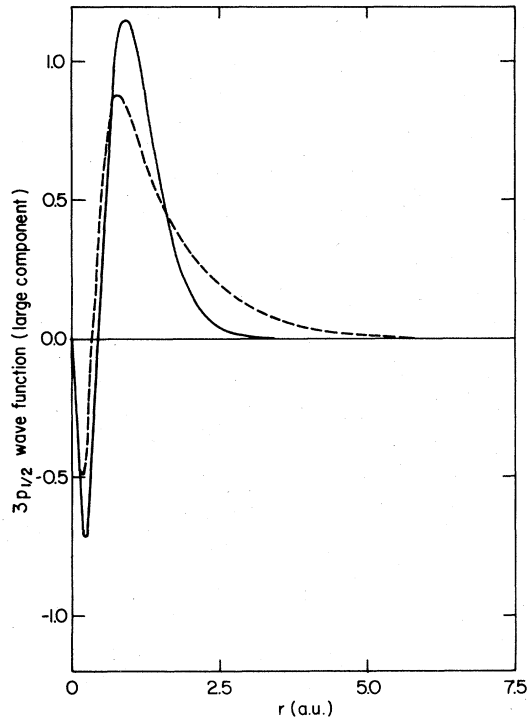

FIG. 4. The large component of the $3p_{1/2}$ wave function of an excited hydrogenlike ion at $n_T=2\times10^{23}$ cm^{-3} (— — —) and for an isolated ion (——).

behavior is a consequence of Eq. (7) whose asymptotic behavior near the nucleus, where $eV(r)\gg\mu$, is $n_f(r)\sim r^{-1/2}$ independent of the plasma density. In spite of the very high density, the integral number of the electrons in this high-density region, however, is very small because of its tiny dimensions.

Figure 3 shows the free-electron spatial distribution around a ground-state H-like ion at constant density, $n_T=2.5\times10^{24}$ cm^{-3}, at three temperatures, $T=200$, 500, and 1000 eV. In fact, this is the temperature range where H-like ions have significant abundance at the given density. It is interesting to note that the main effect of the temperature increase is to flatten the free-electron distribution and to make it more homogeneous, as should be expected on intuitive grounds.

C. Bound-electron wave function

Figure 4 shows the large component of a $3p$ electron wave function of an excited H-like ion for an isolated ion case and when this ion is immersed in a plasma of ion density 10^{23} ions/cm^3. As a consequence of the higher free-electron screening in high-density plasmas, the bound-electron wave function is significantly shifted away from the nucleus. This results in a reduced binding energy. Similar behavior was observed for all the ionic species considered in this paper.

It can be seen in Fig. 4, that there is not much difference between the two wave functions close to the nucleus, and the differences are enhanced with increasing distance from the nucleus. This behavior is a consequence of the accumulated effect of the inner free-electron screening.

D. Binding energies

The variations of the electron binding energies in hydrogenlike, heliumlike, and lithiumlike ions versus density are shown in Fig. 5 (solid lines). These energies were calculated from the eigenvalues of the self-consistent Dirac equation, Eq. (5). For comparison, shown in Fig. 5 are the corresponding variations in a plasma with homogeneous free-electron distribution (dashed lines).

The binding energies are decreasing monotonically with

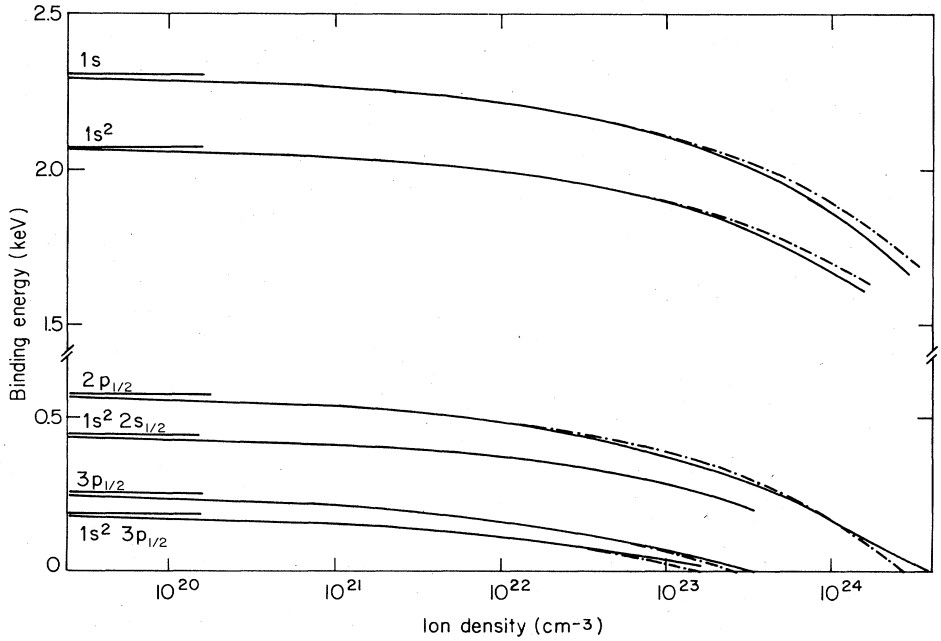

FIG. 5. Binding energies versus density of H-like, He-like, and Li-like species (solid lines). Also shown are the binding energies expected if the free-electron distribution would be homogeneous, Eq. (20) (—·—·—·).

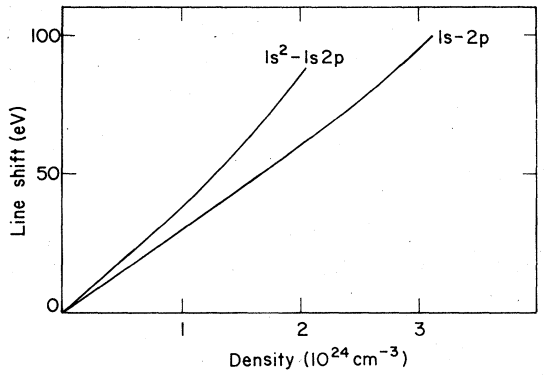

FIG. 6. The shifts versus density of the H-like Lyman-α and the He-like resonance lines.

increasing ion density. This is a result of the screening of the atomic potential by the free electrons which shifts upward the atomic levels. The level shifts are of the order of 40 eV at $n_T=10^{21}$ cm^{-3} up to 200 eV at $n_T=10^{23}$ cm^{-3}.

The shift of the binding energies follows very closely the values predicted assuming a homogeneous free-electron distribution up to $n_T=10^{22}$ cm^{-3}, see Eq. (21). This result suggests that a homogeneous free-electron distribution is a good description of the plasma at low densities up to (almost) solid density, and the level or line shifts can be approximated by the formulas (21) and (24), respectively, with adequate accuracy. Substantial deviations from this behavior can be observed only at higher densities, reflecting the effect of the free-electron polarization around the nucleus in high-density plasma.

E. Line shifts

In Fig. 6 we show the shifts of the H-like Lyman-α and He-like resonance lines versus the plasma density. The line energies were calculated from the eigenvalues of Eq. (3). The lines are all shifted toward the red, as expected on the basis of Eq. (24). The line shifts are of the order of 0.03 eV for $n_T=10^{21}$ cm^{-3} up to 10 eV at $n_T=10^{23}$ cm^{-3}. We recall, however, a point which was already mentioned in the previous section, namely, that the line shift is a second-order effect, and one should be very confident with the accuracy of his model down to second order in order to claim a rigorous result for the line shifts.

A few words of caution are in order. Recently it was proposed that these line shifts may be used to measure the ion-density in highly compressed laser-produced plasmas.[11,13] It should be emphasized that the line shifts are affected by the local instantaneous ion density in the vicinity of the emitting ion rather than the average density in the plasma. This local density undergoes large temporal as well as spatial fluctuations over the whole ensemble. It can be shown[17] that the density fluctuations are of the order of magnitude of the average ion density. Consequently, the spectral lines are not only shifted, but are also broadened, with the linewidth being of the order of the line shift. These line shifts are, therefore, very difficult to verify experimentally except at very low densities.

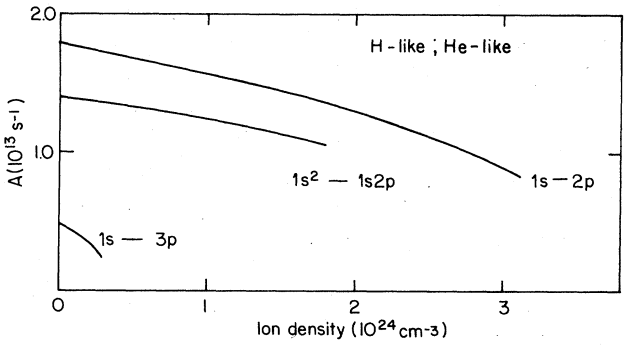

FIG. 7. Ionic transition probabilities of H-like and He-like ions versus density.

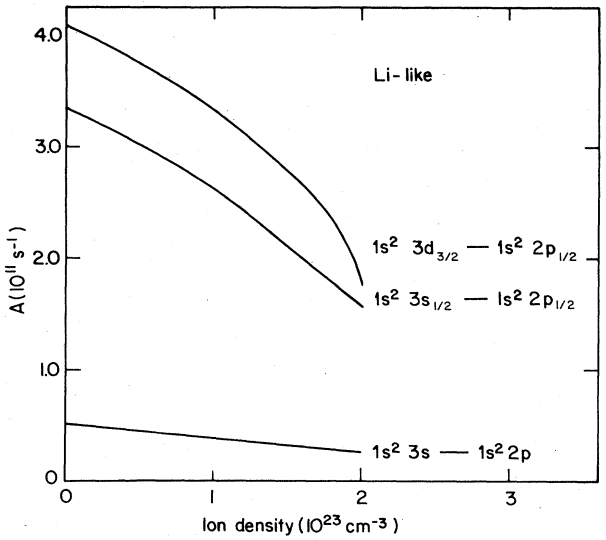

FIG. 8. Same as Fig. 7 for Li-like ions.

F. Transition probabilities

The behavior of the transition probabilities of H-like, He-like, and Li-like species as a function of density are shown in Figs. 7 and 8. These figures are the final results of the present paper.

The transition probability is a monotonically decreasing function of the plasma density. At low densities the deviation of the value of the transition probability from the isolated ion case changes linearly with the density. Only when the upper state approaches its ionization limit does a quadratic term come into effect. Similar behavior would hold true should the free-electron distribution be homogeneous, Eq. (25). When the upper state merges into the continuum, the transition probability finally drops to zero.

C. Dipole-velocity—dipole-length versus density

The longitudinal matrix element, M_{12}^{l} in Eq. (15), vanishes identically for any two states which are the eigensolution of the same Dirac Hamiltonian. In fact, for the

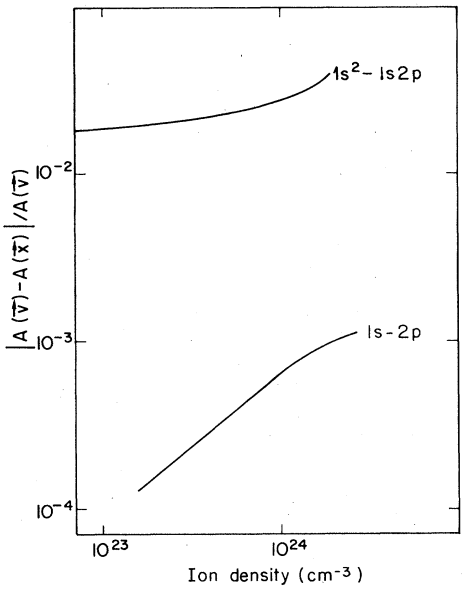

FIG. 9. Density dependence of the relative difference between the transition probabilities of the H-like Lyman-α and He-like resonance transitions as calculated by using the dipole velocity and the dipole length matrix elements.

transition matrix elements in an isolated hydrogenlike ion this condition was satisfied to within the numerical accuracy of our computations. Regarding more complicated ions, as we used relaxed core-type calculation, the upper and lower states were solved in slightly different potentials, so we found differences between the dipole velocity and dipole length transition probabilities even without including the influence of the surrounding plasma.

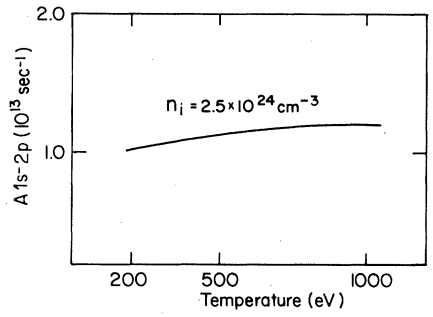

FIG. 10. Variation of the Lyman-α line transition probability with the plasma temperature at $n_T = 2.5\times10^{24}$ cm^{-3}.

The presence of the free electrons in the plasma also affects the difference between the dipole-velocity and dipole-length transition probabilities, see Fig. 9. The origin of this difference is the fact that the free electrons are distributed differently when the ion is in its upper or lower states. The two Hamiltonians are therefore not identical and moreover, their difference increases with increasing ion density.

H. Temperature dependence of the transition probabilities

For comparison purposes we show in Fig. 10 the variation of the transition probability of the $2p$-$1s$ transition in an H-like ion versus temperature between $T=200$ eV and $T=1000$ eV, which is the range where these ions have significant abundance. The ion density is $n_T = 2.5\times10^{24}$ cm^{-3}. Only 20% variation is observed along the whole range. This justifies our concentration on the density rather than the temperature effects of the surrounding plasma.

[1]R. M. More, Atomic Physics in Inertial Confinement Fusion, Lawrence Livermore Laboratory Report No. UCRL-84991 (1981) (unpublished); R. M. More, in *Atomic and Molecular Physics of Controlled Thermonuclear Fusion,* edited by C. J. Joachain and D. E. Post (Plenum, New York, 1983), p. 399.

[2]See, e.g., J. C. Weisheit, in *Applied Atomic Collision Physics,* edited by C. F. Barnett and M. F. A. Harrison (Academic, New York, 1984), Vol. 2, p. 441; D. Mihalas, *Stellar Atmospheres* (Freeman, San Francisco, 1970).

[3]S. Ichimaru, Rev. Mod. Phys. **54**, 1017 (1982).

[4]M. W. C. Dharma-Wardana and F. Perrot, Phys. Rev. A **26**, 2096 (1982).

[5]D. A. Liberman, Phys. Rev. A **20**, 4981 (1979).

[6]R. Cauble, M. Blaha, and J. Davis, Phys. Rev. A **29**, 3280 (1984).

[7]B. F. Rozsnyai, Phys. Rev. A **5**, 1137 (1972); J. Quant. Spectrosc. Radiat. Transfer **27**, 211 (1982).

[8]H. Griem, *Plasma Spectroscopy* (McGraw-Hill, New York, 1964); Phys. Rev **131**, 1170 (1963).

[9]S. Eliezer, A. Krumbein, and D. Salzmann, J. Phys. D **11**, 1693 (1978).

[10]D. Salzmann, R. Y. Yin, and R. H. Pratt, Phys. Rev. A **32**, 3627 (1985).

[11]S. Skupsky, Phys. Rev. A **21**, 1316 (1980).

[12]J. Davis and M. Blaha, J. Quant. Spectrosc. Radiat. Transfer **27**, 307 (1982).

[13]H. Nguyen, M. Koenig, and G. Coulaud, Phys. Lett. **106A**, 34 (1984).

[14]J. C. Stewart and K. D. Pyatt, Astrophys. J. **144**, 1203 (1966).

[15]M. W. C. Dharma-Wardana and R. Taylor, J. Phys. C **14**, 629 (1981).

[16]I. P. Grant, J. Phys. B **7**, 1458 (1984).

[17]D. Salzmann, University of Pittsburgh, Report No. PITT 310, 1983 (unpublished).